Chapter 1

The Impedance Pump

1.1 Introduction

Microfluidics offers an effective means to carry out a wide range of processes within a controlled microenvironment. Much of this appeal comes from the benefits imparted by the surface area to volume ratio of microfluidic systems in terms of reagent consumption and increased transport capabilities. Critical to the implementation of microfluidic devices is the ability to drive fluid within a microenvironment, especially due to that fact microscale flows are often dominated by viscous dissipation. Fluid transport requires the ability to both pump and mix especially where transport must occur over long lengths in short timescales. The pump is therefore an integral component of any microfluidic system. In biological systems, the ability to transport fluid within the microenvironment permits biological systems a means of nourishment and waste removal, in a scientific setting it is a means to manipulate and observe both biological and chemical processes.

The impedance pump has many beneficial characteristics which make it an effective driving mechanism for microfluidic systems. The impedance pump utilizes a bioinspired mechanism for valveless pumping based on resonant wave interactions along a flexible media the therefore can easily be manufactured using current soft lithography techniques. Additionally, the wave based mechanism through which pumping occurs infers many benefits in terms of material choices, lack of moving parts and simplicity in manufacturing. There are no blades, valves or high electric fields required which make the pump safe for studies involving sensitive biomolecules. Adjustment of simple parameters such as the excitation frequency or location can reverse the direction of the flow providing a very versatile range of flow outputs. All of these characteristics make the impedance pump well suited to a variety of applications ranging from active stents and shunts for biomedical implants to providing pumping on demand for microscale thermal management devices, and a modular pump for lab-on-chip diagnostics.

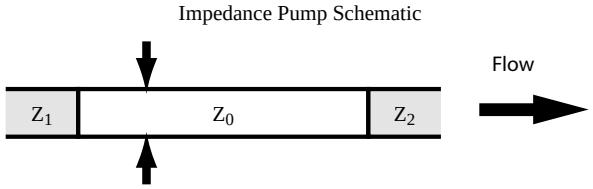

Figure 1.1: A schematic of the impedance pump. The junctions between Z_1 and Z_0 as well as Z_0 and Z_2 form the sites for wave reflection and the arrows represent the pinching location. The system asymmetry is provided both by the difference in length of the excitation from either junction and that the junctions between the different sections may have different wave reflection properties. The impedance pump is reversible, however over the first range of frequencies before any reversal flow would move from left to right in the Figure.

1.1.1 Pump Background

Although impedance based pumping has been known about for some time [1–7] the dynamics are complex and the full potential has not been realized due to the wide number of parameters which can affect performance. We are the first group to begin exploring the potential of impedance pumping as well as to demonstrate it that it is a robust and scaleable concept which can be readily adapted for use biomedical devices and applications in microfluidics [8, 9]. An extensive review of computational and experimental studies can be found in Chapter 1 section 2 of the PhD thesis of Anna Hickerson[10].

1.1.2 Impedance pump concept

1.1.2.1 Principle and Basic physics

The most fundamental principle of its operation is that the excitation occurs asymmetrically with respect to the impedance of the fluid system. The two requirements for an impedance pump in addition to a driving excitation are sites for wave reflection and the presence of systemic asymmetry. Impedance pumps are usually formed by a channel or tube composed of a thin membrane of any material coupled on either side to wave reflection sites. Coupling this membrane at either end to another material or materials of different mechanical properties, geometries or any other factor affecting wave propagation and/or reflection, creates an impedance mismatch, and therefore a site for wave reflection. Commonly, sites for wave reflection are created by changes in material properties and/or geometry and the asymmetry by a change in length. Periodic pinching at an asymmetric location at a certain frequency, waveform and duty cycle results in the accumulation of a pressure gradient from wave interference and therefore the potential to drive flow. A schematic showing the impedance pump can be seen in 1.1.

The concept in brief can be described as follows:

When the compressible section, Z_0 (shown in blue in Figure 1.2), is first pinched down, a pressure wave is emitted in both axial directions traveling at the same speed ($t_1 - t_4$ in Figure 1.2). When a pressure wave encounters a mismatch in impedance, some of the wave will continue to travel through and the rest will be reflected back towards the origin (t_5). In this case the offset in location of the pinching excitation causes the pressure waves interacting with the rigid end segments to reflect at different intervals imposing a phase lag in the reflected wave. The reflected portion of the wave will eventually combine with the next approaching pulse or attenuate out along the length of the compressible section, depending on the selected frequency and duty cycle. The first pressure wave to reflect, headed to the left in Figure 1.2 ($t_2 - t_5$) encounters the wave reflection site and inflects becoming a negative pressure wave which combines with the negative pressure wave created by the restoring force of the compressible membrane drawing fluid in from the left side (t_6). Meanwhile these waves travel to the right until the first wave headed right from the initial compression encounters the boundary moving flow out the right side of the pump before reflecting ($t_7 - t_9$). After the wave reflects it is canceled by the larger negative pressure wave from the inflection continuing to move flow from left to right (t_{10}). The repetition of these dynamic wave interactions under a variety of excitation conditions, wave interference resulting from these out of phase reflections causes the accumulation of a net pressure gradient between the two ends of the compressible section, which in turn interacts with the fluid in the rigid section to establish a mean unidirectional flow. These dynamics have recently been captured and described in computational studies [11]. The impedance pump is bidirectional, however over the first range of frequencies given the asymmetry in the excitation location shown in Figure 1.1 and Figure 1.2, fluid will flow towards the end with the longer length of the compressible section, or from left to right.

1.2 A valveless microimpedance pump driven by electromagnetic actuation

1.2.1 Introduction

Recent interest in microfluidics and microfluidic devices has been predominately driven by the need for biomedical devices on the microscale as well as applications involving chemical control, mixing, and analysis, which stem from the push towards Lab-on-Chip (LOC) methodologies. Micropumping is a necessary component of large integrated systems for sample control and mixing. A micropump requires a compact method of actuation and a mechanism to produce the flow. Commonly micropumps are driven by piezoelectric, electrostatic, electromagnetic, electrohydrodynamic or pneumatic actuators. Mechanisms of pumping vary greatly but can generally be grouped into two categories: displacement pumps and dynamic pumps [12]. These mechanisms can further be categorized in a

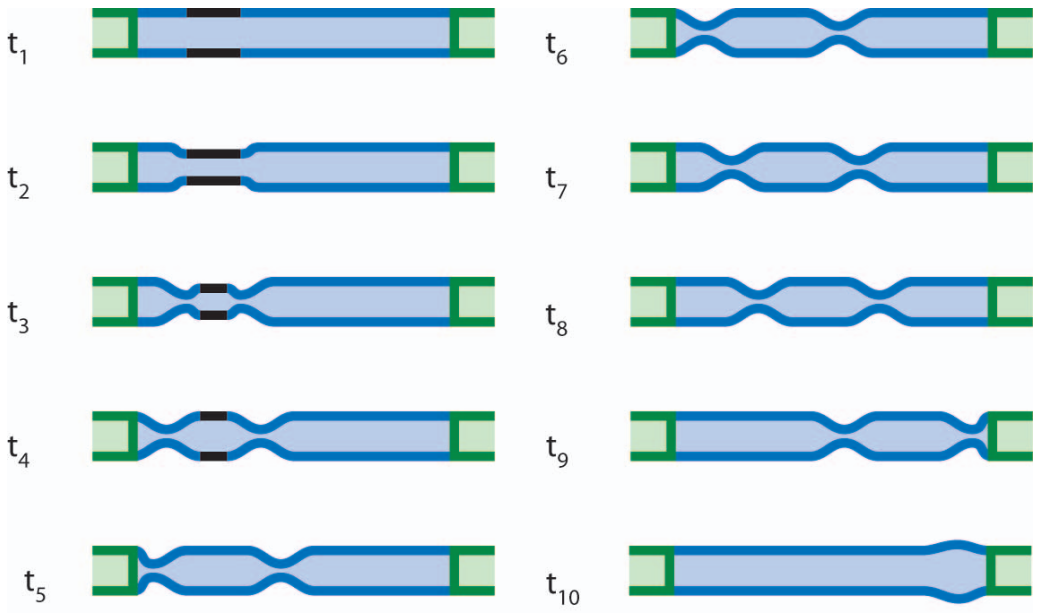

Figure 1.2: A schematic representation of wave interaction along an impedance pump at different time intervals along its length. The wave reflection sites are shown at the ends designated by a color change representing a change in impedance. The black bars indicate where the impedance pump is being excited. Note wave propagate in both directions until they reflect. Observe that due to the asymmetry along the pump length by time step 6 the wave on the right hand side has not reflected whereas on the left hand side the wave is now moving to the right.

variety of ways; one of which is the presence of valves. Conventional valves in microfluidics systems are subject to mechanical failure and, in the case of biological fluids, present further risk of malfunction due to clogging or to damage sensitive biomolecules. Current valveless pumping techniques mainly consist of peristaltic [13] and reciprocating diaphragm pumps relying on diffusers [14–18]. These systems are often fabricated on a substrate through the use of soft lithography on polymeric materials because they are flexible and allow the form and features of these devices to be created and remain functionally sound. Substrate-based systems however, occupy much more volume than is actually required by the device.

Here we present a new valveless and substrate-free impedance based technique for pumping fluid on the microscale. It should be noted that the phenomena resulting in impedance-defined flows has been known for quite some time [1–4, 7]. However, this study is the first of its kind to demonstrate the feasibility of pumping with these phenomena on the microscale, under two different flow circuit configurations, and on two different size scales, as well as report quantitative measurements of the flow performance.

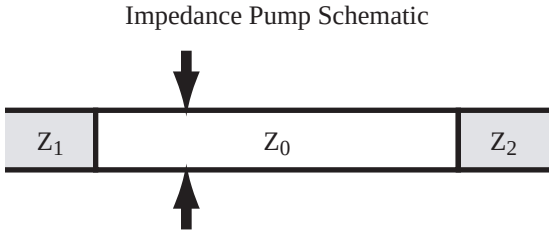

Figure 1.3: A schematic of an impedance pump. The impedances are represented by Z_0, Z_1, and Z_2 respectively. The arrows designate the location of the excitation.

1.2.2 Principle of Operation

An impedance pump is comprised of a compressible section, usually a tube, coupled at both ends to end members of different impedance. Since impedance based pumping is dependent on wave reflection, any material allowing for wave propagation is suitable for the compressible section; in experiments this section is commonly made of a silicone or latex tube. Coupling this flexible tubing at either end to another material or materials of different mechanical properties, geometries or any other factor affecting wave propagation and/or reflection, creates an impedance mismatch, and therefore a site for wave reflection. In Figure 1.3, which depicts a schematic of the pump, these impedances are represented by Z_0, Z_1, and Z_2. The most fundamental principle of its operation is that the excitation occurs asymmetrically with respect to the impedance of the fluid system. Periodic pinching at an asymmetric location at a certain frequency, waveform and duty cycle results in the accumulation of a pressure gradient from wave interference and therefore the potential to drive flow.

In our experiments this system takes the form of a thin walled elastic tube coupled at either end to two symmetric segments composed of a less compliant material, glass, and filled with water. Since the glass segments are of equal impedance the asymmetry must be caused by the location of the excitation along the length of the elastic tube. The difference in length over which the waves travel before reflecting imposes a phase difference in the traveling waves returning to the excitation site. Neglecting attenuation and the effects of viscosity for simplicity, one could imagine conditions where at a certain frequency or band of frequencies the interference of reflecting waves traveling in both directions can form pressure gradients and induce flow. Through the complete collapse of the elastic section the system can also function as a valve.

1.2.3 Experimental setup

For the remainder of this paper the following distinction will be made. Open loop will be defined as flow between two independent reservoirs on both sides of the pump, with no fluidic interconnections. Closed loop will be defined as flow within a distinct loop. Previously, the behavior of the impedance

Configuration	Tubing dimensions ID/wall	Material	Actuation type
Closed loop	2 mm / 50 μm	Silicone	Perpendicular (Fig. 1.5)
Open loop	2 mm / 50 μm	Silicone	In-line (Fig. 1.6)
μOpen loop	250 μm / 50 μm	Polyurethane	Perpendicular (Fig. 1.5)
Device	2 mm / 50 μm	Silicone	In-line (Fig. 1.6)

Table 1.1: A summary of the impedance pump testing configurations including actuation type and dimensions based on the testing configuration.

pump has been studied in both of these configurations at larger size scales [8]. In this study, the impedance pump was tested under three configurations spanning two different size scales: closed loop, open loop and micro open loop. For these configurations, two different electromagnetic actuation schemes were devised referred to as perpendicular and in-line, specifying their orientation with respect to the axis of the fluid channel. A device was also created demonstrating the feasibility of packaging a majority of the pump components into a free-standing micro pump. Table 1.2.3 summarizes the configurations and their respective electromagnetic actuator types. In all cases the glass sections attached to the micro pump are symmetric, and therefore equal in impedance. As a result of this symmetry, excitation at the midline of the elastic tube produces no net flow.

The thin walled elastic tubes used for the pump in the open loop and closed loop experiments were made of silicone with a Young's modulus of 0.4 MPa (at 100% elongation), an inner diameter (ID) of 2 mm and a wall thickness of 50 μm. The tubing used in the micro open loop study was made of polyurethane with a Young's modulus of 2 MPa (at 100% elongation), an inner diameter of 250 μm and a wall thickness of 50 μm. Unless otherwise mentioned, the elastic tubing was connected to glass tubing with an inner diameter of 0.8 mm and a 0.6 mm wall. All impedance pumps constructed using the tubing mentioned in the previous sentence were sealed on either end to the glass tube using heat shrink. A diagram of the assembly procedure can be seen in Figure 1.4.

1.2.3.1 Micro impedance pump actuation

Although any technique could have been employed, electromagnetic actuation was chosen because of its large displacement, high frequency capabilities. Two different electromagnetic actuation schemes were examined, one for experimental purposes, and the other for device oriented studies, shown in Figure 1.5 and Figure 1.6 respectively. Actuation was achieved by fixing a Neodymium Iron Boron (NdFeB) rare earth magnet cube with a side length of 2.4 mm using silicone glue to the upper surface of the tube at an asymmetrical location along the elastic tube length. This magnet was oriented such that when the coil was energized their magnetic field gradients produce a radial force compressing the tube. In the first configuration, the magnetic field of the magnet was oriented such that when the coil was energized its poles are parallel to those of the permanent magnet. A schematic illustrating the

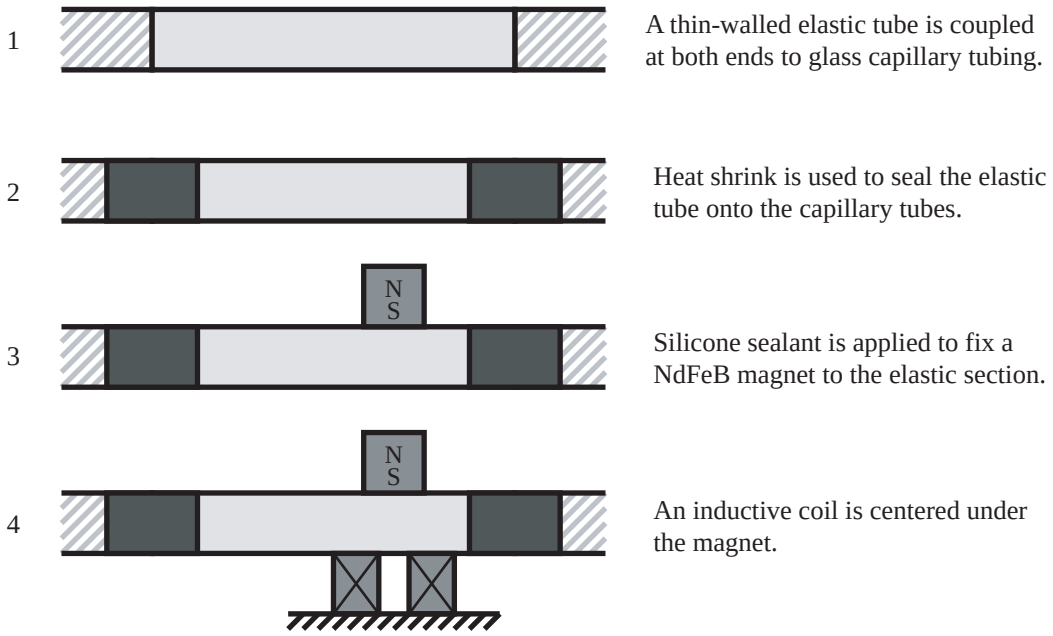

Figure 1.4: A diagram showing the assembly of an electromagnetically actuated impedance pump.

inductor-driven electromagnetic actuator in a perpendicular configuration can be seen in Figure 1.5. The second actuation scheme takes advantage of the fact that fluid passages in biological systems as well as medical devices are generally cylindrically symmetric in shape. To conserve space as well as complement the symmetry of the tube, a novel inline coil-magnet configuration was created comprised of two coils wound azimuthally symmetric with respect to the elastic tube and connected such that when energized they are in-phase. A compressive radial force can therefore be generated by locating a permanent magnet element equidistant from both coils with its magnetic pole oriented such that it is parallel to the length of the tube. A diagram of the inline coil-magnet configuration can be seen in Figure 1.6.

1.2.3.2 Closed Loop Flow

The closed loop test section was formed by coupling a thin walled elastic tube to one end of the two symmetric sections of the glass flow loop. The fluidic loop was completed by connecting the opposite ends with a latex tube with a significantly thicker wall, making it much more rigid than the elastic tube of the pump but soft enough to be crimped, isolating one section from the other. Crimping this thicker elastic tube closes one section off from the other, and creates an open loop situation in which a pressure differential can be measured between the water levels on either side of the pump. Each section also has a piece of glass tubing connected perpendicular to the plane of the flow loop on the

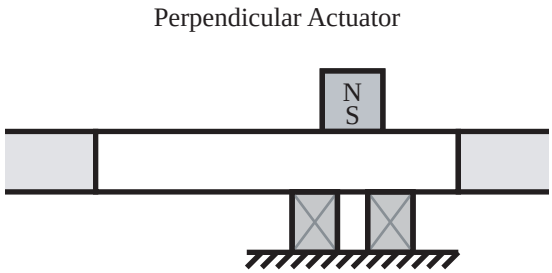

Figure 1.5: Schematic showing an impedance pump with inductance driven actuation in the perpendicular configuration. The letters N and S designate the orientation of the permanent magnet poles.

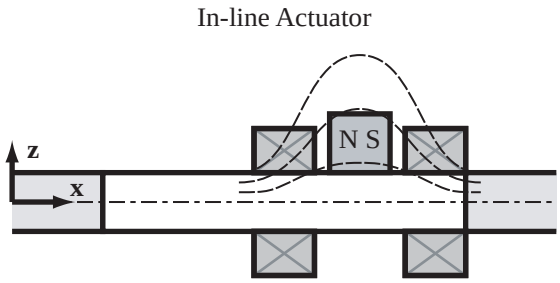

Figure 1.6: A schematic of the inductive coils wound in the in-line azimuthally symmetric format parallel to the x-axis along which flow occurs. The letters N and S designate the orientation of the permanent magnet poles.

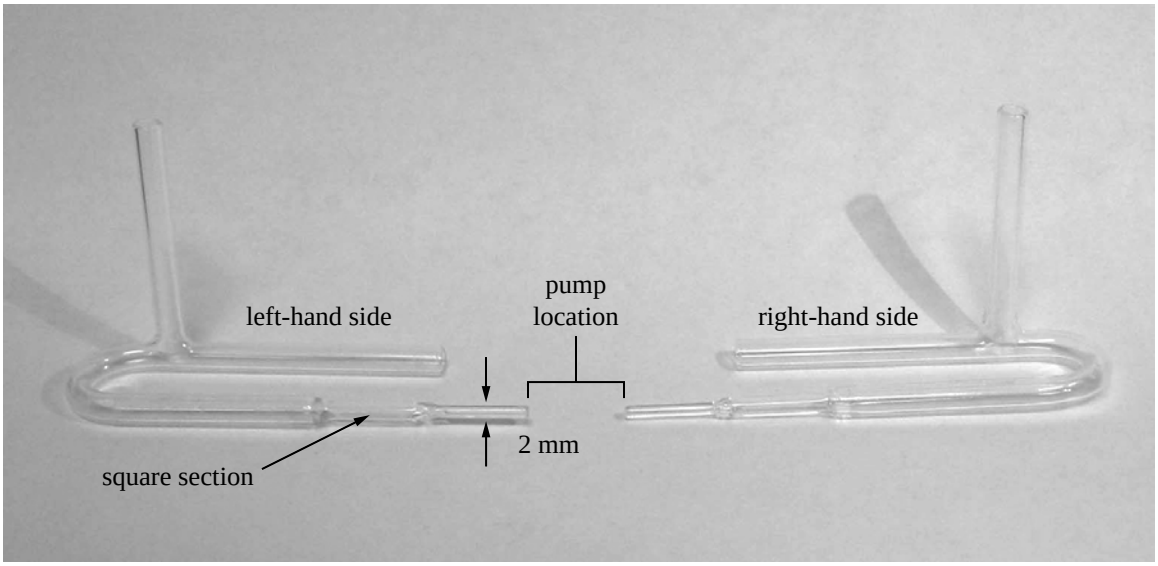

Figure 1.7: A picture of the closed loop flow circuit glass pieces. Also shown is the square section where flow velocity is measured. In operation the pump is attached between the two sides of the loop closest to the reader with an outer diameter of 2 mm. For measurements, clockwise flow within the loop, from the right-hand side to the left hand side, was taken as positive.

opposite end of the pumping site. The inner diameter along a majority of the length of the glass flow loop is 3.2 mm. On one end the tubing of the loop tapers to accommodate a 2 mm side-length square section, where the flow rates can be measured. The square section is then connected to a smaller diameter glass tube (0.8 mm ID, 0.6 mm wall) that connects the loop to the elastic tube. Figure 1.7 shows a picture of the closed loop flow circuit. In this configuration, energizing an inductive coil positioned under the magnet allows the tube to be compressed forming the pump. A schematic of the actuator can be seen in Figure 1.6. Measurements of the bulk flow velocity were taken using a Viosense Mini Laser Doppler Velocimetry (LDV) system, through the length of square tubing on the flow loop. The fluid was seeded with 3 μm neutrally-buoyant polystyrene microspheres. The best results were achieved with particles equal to or less than the fringe spacing ($\sim$ 11 μm) of the LDV. The Mini LDV has 97 % accuracy and a repeatability uncertainty of 1%. Important parameters for reliable measurements and to prevent the particles from adhering to the glass flow loop were the particle size, material, and buoyancy.

1.2.3.3 Open Loop Flow

In a device driven study similar to the environment under which a medically implantable device may operate, the inflow to the device may not contain returning fluid inertia. Open loop flow was therefore demonstrated by connecting the silicone tubing to a short length of the glass tubing (0.8 mm ID, 0.6 mm wall) through the procedure described in Figure 1.4 and placing either end into two independent water reservoirs of a known volume, dispensed through a micropipette. Flow rates were

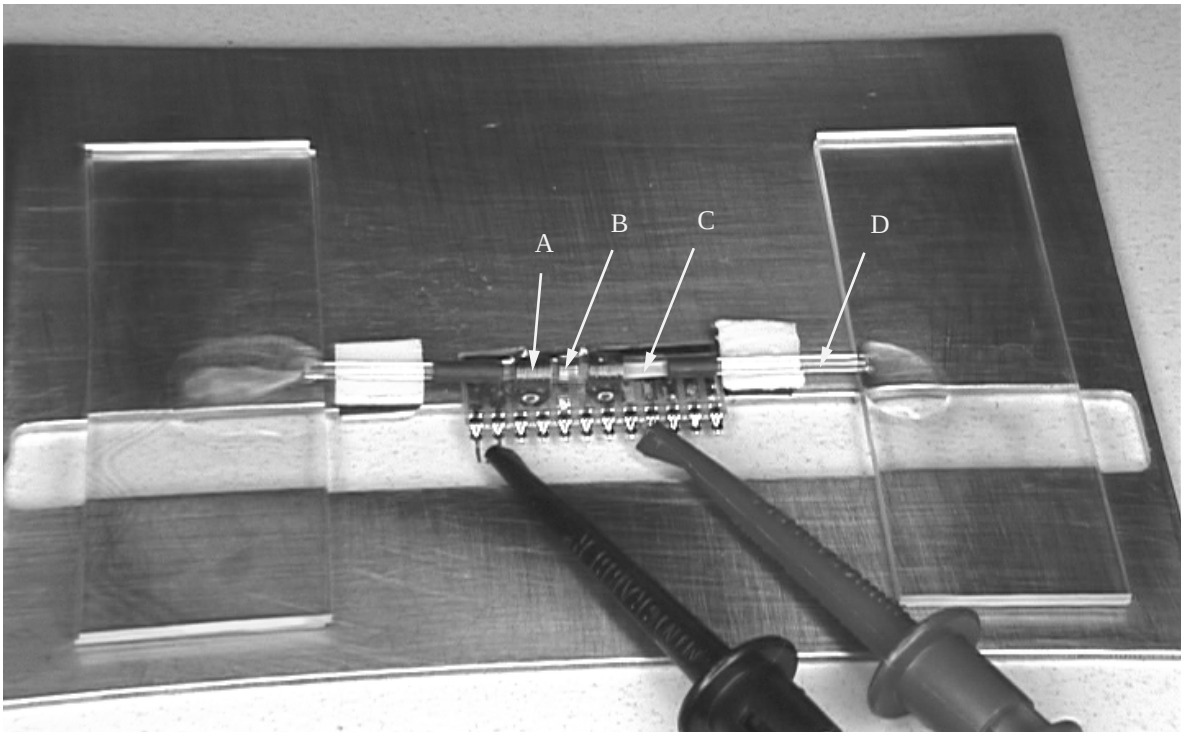

Figure 1.8: Shows the functioning pump in the open loop configuration employing the in-line actuation technique. The letters A, B, C, and D denote the coil, magnet, silicone tube and glass tube, respectively. Fluorescein dye has been used to visualize the movement of fluid from one reservoir to the other. The Teflon slides have been removed for clarity.

determined by measuring the time required for the pump to consume the entire droplet. To prevent capillary action from drawing the fluid along the bottom of the tube, the ends of the glass tubing were placed on two glass slides disconnected from the pump as well as each other. In addition, polytetrafluoroethylene (PTFE) rectangles were stuck to the slides using double-sided tape. The hydrophobicity of PTFE facilitates the visualization of the droplets. An image of such an assembly can be seen in Figure 1.8.

1.2.3.4 Micro Open Loop

The micro open loop flow experiment was constructed by pressing a short length of glass capillary tubing into either the end of the elastic section. In this case, heat shrink was not required to seal the coupled tubes, as described by the procedure above. Similar to the larger open loop study Teflon coated slides were used to visualize the flow of droplets of known volume from one side of the pump to the other. The excitation in this case was provided by cantilever style actuator based on the in-line electromagnetic scheme. A picture of the micro open loop test assembly can be seen in Figure 1.9.

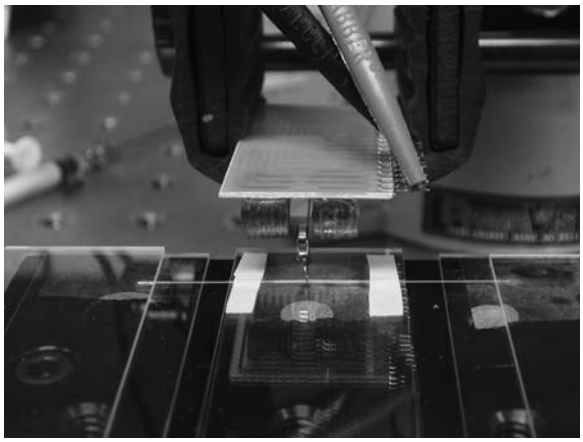

Figure 1.9: Picture of the micro open loop configuration showing the elastic section, glass tubing and actuator. The PTFE slides are not present so the glass tubing is visible.

1.2.4 Results

1.2.4.1 Closed Loop

The closed loop flow response of the impedance pump was observed to be reversible as well as highly dependent on frequency. The performance of the pump was found to be very sensitive to the waveform, offset, amplitude and duty cycle of the excitation. A typical frequency response can be seen in Figure 1.10. Clockwise flow, into the right hand side of the elastic tube was taken as positive. The magnet was located at 4.2 mm from the right hand side of a 19.6 mm tube length. The input waveform to the coil was a square waveform, 48 mA in amplitude, with a 16 mA offset and a 50% duty cycle. Consistently there was at least one flow reversal as the frequency was increased. Figure 1.10 shows three such reversals. These can be seen to occur at roughly 21 Hz, 89 Hz, and 142 Hz. Although similar net flow rates were observed at both high and low frequencies, at low frequencies the flow was highly oscillatory. As the frequency of excitation was increased, bulk flow oscillations tend to damp out resulting in unidirectional flow. Flow rates of up to 16 mL/min have been achieved. For the curve shown in Figure 1.10 the maximum flow rate was 11 mL/min at 55 Hz corresponding to a Reynolds number (Re) of 730.

1.2.4.2 Open Loop

For the open loop configuration the magnet was located 7.25 mm from the end of the 19.14 mm. The input to the coils was a 60.7 Hz a square wave 200 mA in amplitude with no offset. Flow rates exceeding 191 μL/min were achieved pumping a 100 μL droplet to the opposite end of the pump, corresponding to a Re of 5. Relatively high flow was achieved despite the fact that, in this setup, the magnet does not in any form compress the tube against a fixed opposing surface. A demonstration of flow in the open loop configuration can be observed in the sequence of frames pictured in Figure

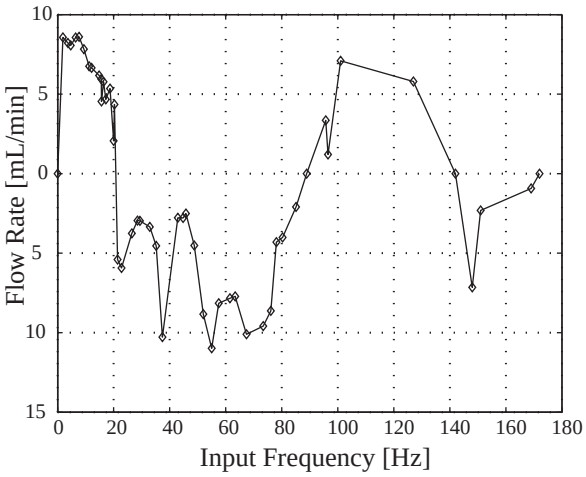

Figure 1.10: A typical frequency flow response of an impedance pump, comprised of an elastic section with an inner diameter of 2 mm and wall thickness of 50 μm coupled at either end to glass tubing of 0.8 mm in inner diameter and 0.6 mm wall thickness excited 4.2 mm from the end of the loop first to see clockwise flow.

1.11. In this sequence of frames a drop of fluorescein dye was used to visualize the flow of fluid across the pump.

1.2.4.3 Micro Open Loop

Since viscosity tends to dominate on the microscale, a study was done to determine whether impedance defined flows still function at very low Re. Tests were performed in the open loop configuration described above using a polyurethane (PU) tube, with a 250 μm inner diameter and a 50 μm wall thickness coupled to a borosilicate glass capillary tube with a 150 μm inner diameter and a 50 μm wall thickness. PU was chosen due to its large tensile strength when compared to most elastomers enabling smaller inner diameters and wall thicknesses than would otherwise be possible. Using an 82.0 Hz excitation and water as the fluid, flow rates were measured to be approximately 17 μL/min or a $Re \sim 2$. The pressure gradient created by the pump was large enough to expel droplets out of one end of the test assembly. In this configuration flow has been shown to be highly frequency dependent and reversible.

1.2.4.4 Description of the micro impedance pumping device

Currently, the design of the micro impedance pump has focused on creating a free standing device that does not rely on a supporting glass or polymeric substrate. The chosen geometry for the compressible section was a tube. Therefore, to create a freestanding device, a titanium cage was manufactured using conventional micromachining techniques. The two major factors that weighed into the design the micro impedance pump cage aside from those inherent in its principles were

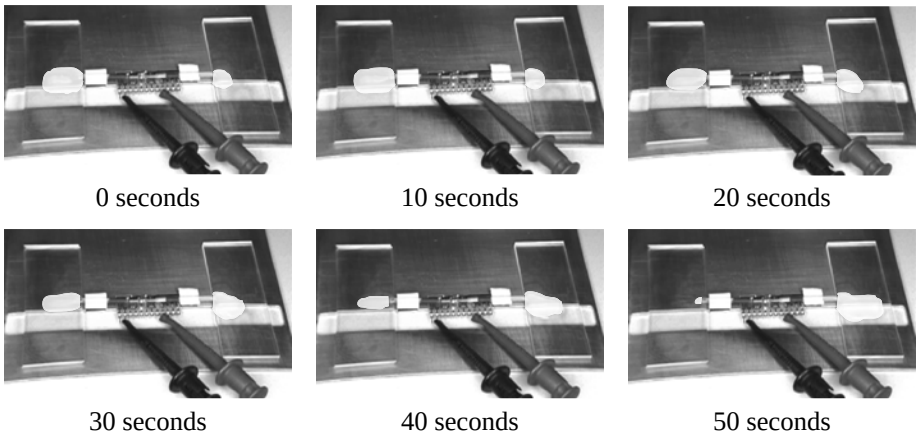

Figure 1.11: A sequence of photos demonstrating functionality of pumping fluid open loop, using the inline actuation type. The puddle on the left can be seen to contain a spot of fluorescein dye. At t = 0 seconds a square current waveform of 200 mA in amplitude at 60.7 Hz was input to the coils. Over a 50 second duration following the current input, the fluid containing the drop of dye was pumped from the slide on the left to the slide on the right.

the structural integrity of the elastic tube, and providing a compact means for the excitation. A thin wall, although beneficial to wave propagation, often meant that the tubing was collapsible and therefore required some structure to prevent buckling or collapsing. In addition, the way in which the tube was coupled to the cage was important to prevent tearing, and ensure the lifetime of the device. For the device pictured in Figure 1.12, the tubing was turned inside out and stretched over the cage, then fixed using heat shrink.

1.2.5 Discussion

High frequency excitation revealed the presence of multiple regimes of flow. The upper limit of this excitation was only limited by the attenuation of the magnetic field gradients produced by the coil at high frequency, consequently changing the excitation profile. Flow in all cases was observed to be highly dependent on frequency, waveform, duty cycle and amplitude of the input excitation. The reliance of impedance driven flows on the type of excitation provides some evidence for the occurrence of wave-based interactions being cumulatively responsible for the manifestation of flow. The dependence of the flow rate on frequency can easily be observed in the plot in Figure 1.10. Wave interference also offers some explanation as to why there was consistently a flow reversal. The presence of the elastic section implied there was at least some phase delay between the pressure and velocity waves produced with each excitation. The flow reversals as well as the flow peaks most likely correspond to frequencies where the phase delay between the reflecting waves and the source waves was the least and most optimal, respectively. The vast frequency range for which flow occurs allows for the selection of completely different, application specific flow regimes with just one pump.

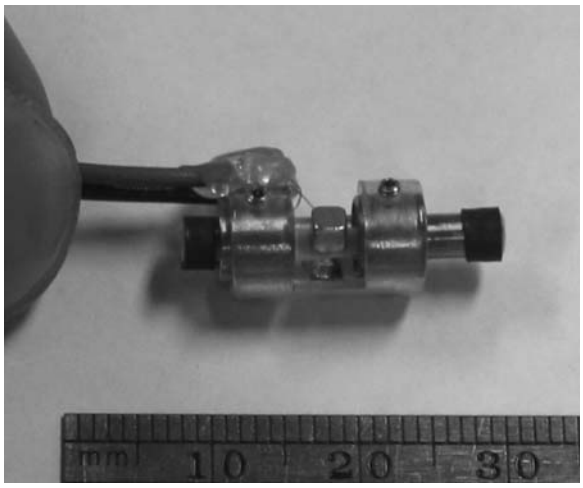

Figure 1.12: A picture of the free-standing micro impedance pump.

Functionality in the open loop configuration is also significant. In essence the inertia of the returning flow is not required to maintain pressure or flow. Instead, solely the presence of an impedance mismatch and asymmetric excitation are required to generate a pressure gradient at certain frequencies. The flow rates in either case differ by two orders of magnitude. As reported above, the micro impedance pump in the closed loop flow configuration has attained flow rates of up to 16 mL/min, whereas in the open loop configuration under similar parameters maximum flow rates have consistently been much lower ($\sim$ 191 μL/min). In contrast to other mechanisms of pumping, the increased system impedance in the closed loop configuration may actually benefit the impedance pump's performance.

1.2.6 Conclusion

Impedance based pumping has been shown to be a viable method for moving and controlling fluids on the microscale. High frequency electromagnetic actuation has revealed multiple regimes of performance which can easily be controlled as well as reversed by simply varying the frequency of excitation. As a result, micro impedance based pumping can deliver both high and low flow rates under a variety of pressure conditions. Flow rates of 16 mL/min and 191 μL/min have been demonstrated in the closed loop and open loop flow configurations respectively. In the micro open loop trials flow rates as high as 17 μL/min have been achieved. These numbers position the micro impedance pump flow performance significantly ahead of the flow rates achieved using other micro pumping mechanisms with similar dimensions.

The performance of the micro impedance pump has been observed to be dependent on a variety of parameters, namely the duty cycle, frequency, and amplitude of excitation as well as the fluid-mechanical properties of the system. However, adjusting one parameter, such as the frequency,

Table 1.2: Summarizes the parameter space of the impedance pump. **Note**: Many of the material and geometrical parameters should be considered as counting twice since they describe the compressible section of the pump and the rigid end connections.

Material Properties	Fluid Properties	Actuation	Geometry
Young's modulus	Viscosity	Shape of actuator	Length
Reflection coefficient	Pressure	Waveform	Inner diameter
Wave speed	Flow Resistance	Location	Wall thickness

enables the device to be readily tuned to achieve the desired performance. The micro impedance pump is relatively easy to construct and does not require any complex fabrication methods to build and operate. The micro impedance pump is highly resistant to clogging due in part to the pulsatile nature of the flow as well as the lack of diffusers and valves. The presence of flow in the absence of complete closure of tube, in both the open loop and closed loop configurations, may prove to be beneficial for the handling sensitive biofluids. In addition to its substrate free construction, the absence of complex parts and inner geometries makes the impedance pump well suited for integration into cost focused, space limited applications including drug delivery, cell sorting, chemical analysis, as well as act to complement current stenting and shunting techniques. Micro impedance based pumping presents an exciting new method of controlling fluids on the microscale with vast potential in a variety of applications, especially with respect to micro mixing as it relates to chemical or biological assays (DNA Chip). Although it is conceptually simple, significant future work is necessary to be able to further understand and predict the complex dynamics of impedance driven flows.

1.3 Characterizing the impedance pump

1.3.1 Introduction

The study of the electromagnetically actuated valveless microimpedance pump demonstrated the need to decouple the actuator from the pump body. Although this study was a demonstration of the ease to which impedance pumps can be implemented at the small scale the results represent the performance of two unoptimized systems. The study also elucidated the difficulties presented in comparing one pump to the next in terms of frequency response due to the large parameter space which gives rise to the pump flow output. Since the impedance pump has such a large parameter space based on material, geometric and excitation parameters it was necessary to construct an experimental system which would allow the freedom to explore the pump dynamics in a variety of configurations. The parameter space for the pump is summarized in Table 1.2. Additionally the construction of the pump mainly the limited force output and the gluing of the electromagnetic actuator prevented the exploration of the full parameter space.

Since our working hypothesis about the physics of the impedance pump was based on the interaction of pressure and velocity waves inside the body of the pump it was necessary to have measurements of the time resolved flow rate and pressure. Phase information about these pressure and velocity waves at different frequencies allows a picture of how wave interactions give rise to pumping. Since directly taking the measurement inside of the pump is not an option both pressure and flow rate were measured downstream of the pump relying on the fact that the phase relationship between the pressure and velocity waves does not change in a system with rigid boundaries.

1.3.2 Experimental Setup

An apparatus was therefore constructed to examine the flow dynamics of the impedance pump in a variety of different configurations. A schematic of the experimental setup can be seen in Figure 1.13. A Bruel and Kjaer 4810 voice coil actuator was chosen to provide large displacement, high frequency actuation at up to 10 N of force. A voltage to current amplifier was constructed to provide up to 1.8 A_{rms} or current from DC to 10 kHz. The voice coil was mounted vertically on a 3-axis micrometer stage. Position adjustments in all three directions allow for the following: transverse centering of the excitation relative to the pump body, fine adjustment of the excitation position over the entire length of the pump and adjustment of the excitation location into the pump body. The ability to adjust into the z-depth gives the apparatus the freedom to test impedance pumps of a wide range of diameters as well as ensure the excitation always remains in contact with the pump body. The displacement of the voice coil actuator is transmitted to the pump through a probe. Inset in the probe is an LVDT core, which provides displacement information about the probe through an LVDT. The probe then tapers to a 2.4 mm diameter circular surface which makes contact with the pump body. The transfer function relating displacement to frequency for the electromechanical system comprised of the voltage to current amplifier, voice coil actuator, and probe was recorded using an HP Dynamic Signal Analyzer and a transfer function was created to provide open loop control of the probe displacement. This transfer function can be viewed in Appendix B.

A two piece flow loop was also designed, the matching sides of either half providing rigid boundaries as part of the impedance pump, and a means to inserting the ultrasonic transducer into the flow loop, respectively. In addition either half has two ports which emerge perpendicular to the flow plane. Two are located on either side of the pump boundaries for a differential pressure measurement of pump output. The other two ports provide an easy means to flush the system and remove any bubbles. Dynamic flow rate measurements at low flow (μL/min to mL/min) rates are particularly difficult to measure with accuracy and sufficient bandwidth. An ultrasonic probe Transonic ME-2 PXN was chosen to provide real time flow rate measurements up to a frequency of 150 Hz with minimal end user processing. This probe is compatible with a number of fluids in particular glycerin giving the experimentalist the ability to vary the fluid viscosity.

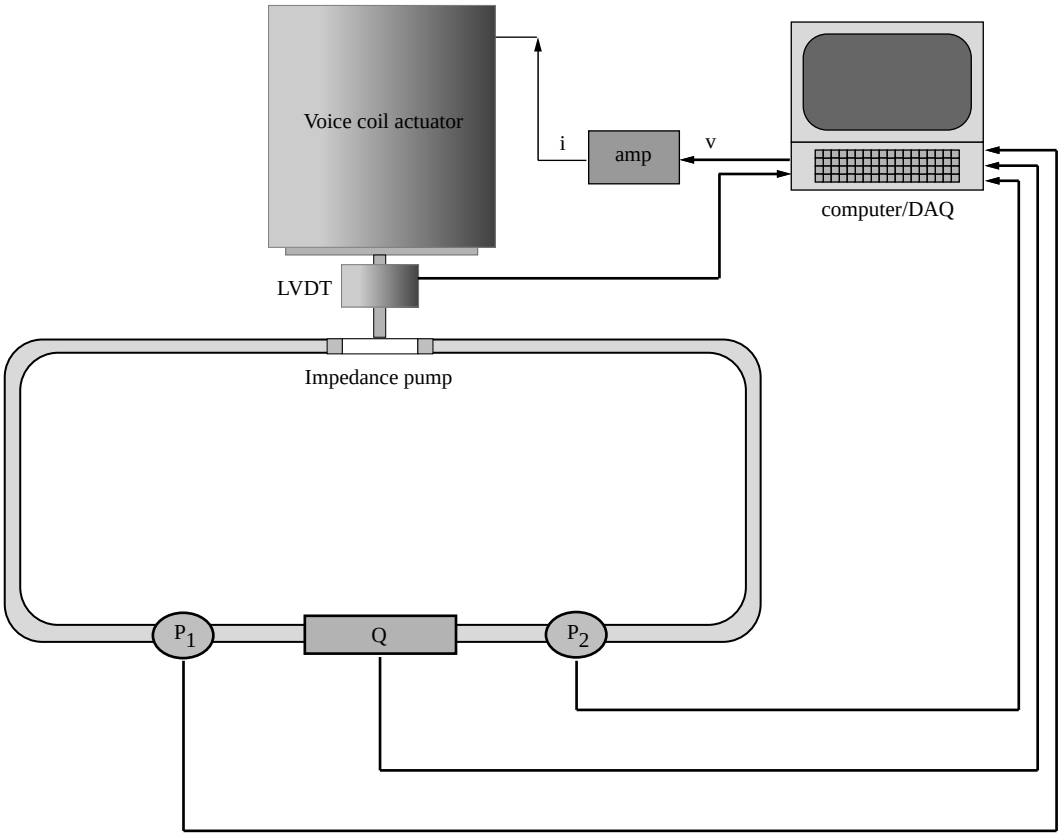

Figure 1.13: A schematic of the impedance pump characterization system. The voice coil is used to provide an excitation to the pump, the LVDT is present to measure the amplitude of the excitation. Pressure and flow were monitored by two differential pressure transducers (P_1 and P_2) and a flow meter (Q) respectively.

Time resolved fluid pressure measurements at small size scales are particularly difficult due to the fact that they are based on a stagnation pressure and the diaphragm is often many characteristic diameters away from the main channel flow. Undoubtedly the amplitude of the dynamic portion of the pressure measurement is attenuated by this affect. Most pressure measurement techniques rely on large surface area diaphragms for capacitive measurements however they are usually many times larger than the experimental system itself making coupling difficult. Silicon piezo-resistive pressure transducers were therefore chosen due to their small size, sufficient sensitivity and high bandwidth (1-3 msec). A table summarizing the technical specifications of all the various components can be found in Appendix A.

1.3.3 Results

1.3.3.1 Pressure and Flow versus frequency

The construction of the experimental apparatus provided data further demonstrating the importance of wave dynamics in the performance of the pump by providing the first empirical evidence of time resolved pressure and flow of a wide range of frequencies with a controllable waveform. The plot in Figure 1.14 shows a typical frequency response of an impedance pump tested using characterization setup. The pump was comprised of a silicone tube 20 mm in length, 2 mm in inner diameter (ID) with a 780 μm wall, coupled to two glass capillary tubes 2 mm in outer diamter (OD) and 1 mm in ID. Unlike that shown in Figure 1.10 from the LDV the frequency response is smooth due to the sampling rate of the ultrasonic transducer. Also evident from the simultaneous pressure and flow measurements is that both the maximum pressure and maximum flow occur at the same frequency demonstrating the resonant behavior of the impedance pump. In other words maximum mechanical power is transmitted to the working fluid at a specific frequency. This particular behavior was also noticed in the larger scale impedance pumps. Additionally this data represents the first empirical study to measure both the pressure and flow frequency response simultaneously to hundreds of Hertz in a closed flow loop configuration.

1.3.3.2 Impedance pump flow response versus position

Another experimental parameter relevant to characterizing the pump, provided by the new experimental setup, was the ability to examine the pump flow response versus position. Figure 1.15 shows the response of a 2 mm ID, 20 mm in length pump over a range of positions spanning 4.5 mm to 15.5 mm in 0.5 mm increments. Stepping left to right across the length of the pump produces the symmetric plot shown in Figure 1.15. The symmetric flow response of the pump to changes in the position of the excitation is another demonstratration of the wave based behavior of the pump physics another trait of impedance pumps of all size scales. As in all cases presented so forth both

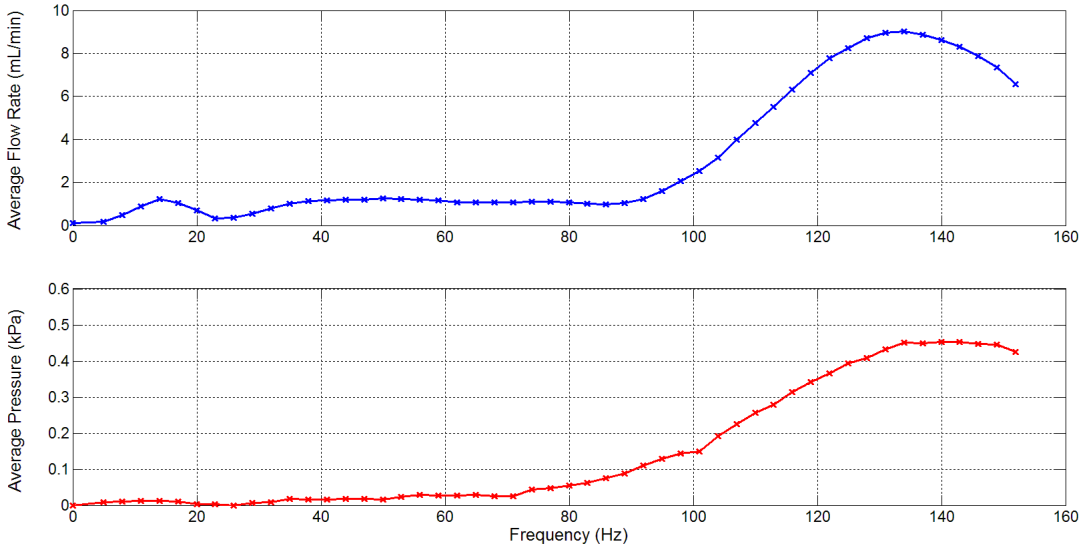

Figure 1.14: Shows a typical flow and frequency response for a millimeter scale impedance pump. The plot shows that both pressure and flow peak at the same frequency representing maximum power transmission to the fluid.

boundaries are the same so asymmetry is purely applied by change in offset position. If the excitation is located in the center the pump produces no flow since the pressure difference produced on either side of the pump cancels the other out. As the excitation location increases in asymmetry for example moves closer to one impedance mismatch boundary or the other the resonant peaks in the flow response increase.

1.3.3.3 The phase relationship between pressure and flow

The fabrication of this new setup also enabled us to examine the interaction between transient pressure and velocity waves inside of the pump. These results are illustrated in the following pressure-flow loops (P-Q). Figure 1.16 shows the frequency response of the pump from which the flow and pressure time traces were recorded. Three points are labeled on this figure denoting the various frequencies examined in Figure 1.17 - Figure 1.19. Figure 1.17 - Figure 1.19 show the phase relationship between pressure and flow at three frequencies around resonance as well as the representative P-Q loops. At 116 Hz it can be clearly seen that the pressure precedes flow in time. At this frequency the phase lag produces an open clockwise rotating P-Q loop. As the frequency is increased towards resonance at 134 Hz, it can be seen in Figure 1.18 that both pressure and flow are in phase and accordingly the P-Q loop collapses. As the excitation frequency passes over 134 Hz the P-Q loop opens up and inflects producing a counterclockwise rotation as pressure trace now lags behind the flow trace in time. This behavior can be observed in Figure 1.19 at 152 Hz.

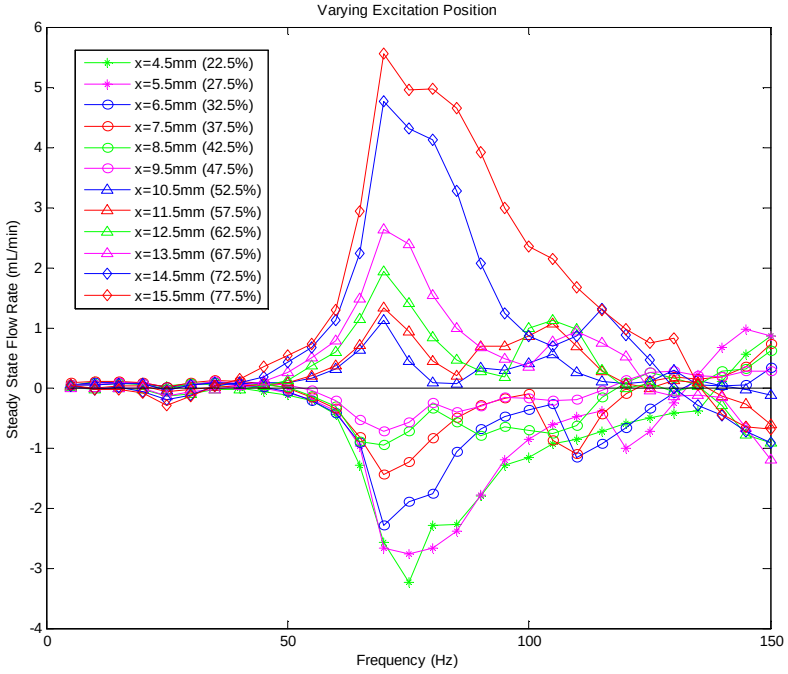

Figure 1.15: The flow response of an impedance pump translating the excitation location from left to right across the length of the body of the pump. The resonant frequency is clearly observable at 72 Hz and is persistent regardless of the position of the excitation. Note: Positive flow is denoted counterclockwise.

1.3.4 Discussion

The characterization of the millimeter scale impedance pump allowed a confirmation of many of the traits of the larger scale ($\sim$ 2 cm) impedance pumps studied by Hickerson in her thesis namely the simultaneous occurrence of peak pressure and peak flow at a single resonant frequency, the persistence of resonant frequency regardless of excitation location, the symmetrical response of the pump to the center location of the pump tube as well as the collapse of the P-Q loop at resonance. The peak flow of around 10 mL/min is typical for impedance pumps around 2 mm in inner diameter, with a typical maximum static pressure head of around 20 kPa.

The pressure-flow time traces also showed a similar behavior to larger scale impedance pumps. Spanning the resonant peak of the frequency response at close to 134 Hz, the open P-Q loops shown in Figure 1.17 and Figure 1.19 at frequencies of 116 Hz and 152 Hz respectively demonstrate how pressure and flow interact to give rise to conditions of maximal flow. The clockwise open loop at 116 Hz and the counterclockwise loop at 152 Hz represent fluid mechanical power not being transmitted to the flow. The subsequent collapse of this loop near resonance at 134 Hz represents full power transmission to the fluid in terms of mean flow as well as static pressure head.

1.3.5 Conclusion

The construction of the characterization apparatus greatly improved the parameter space which could be explored for a single pump. Improvements to the actuation and instrumentation enabled data to be acquired more quickly as well as a versatile platform for testing pumps of many different size scales. The improvement to the flow data is clearly evident in comparing Figure 1.10 to Figure 1.14. The combination of the voice coil and LVDT allowed for open loop control of the displacement and position information about the actual displacement of the voice coil probe at frequencies up to 160 Hz, an order of magnitude larger than any previous experimental study. The combination of the pressure transducers and ultrasonic flow velocity probe allowed for rapid measurements of pressure and flow allowing the large frequency space up to 160 Hz to be spanned accurately accommodating the dynamic flow response of the pump where changes of a few Hertz can result in flow spikes, flow reversals or both. The apparatus also allowed for the observation of key features of the flow dynamics of the impedance pump relating the pressure to the flow in time and how their relationship in phase gives rise to flow. However the exact dynamics and interaction of pressure and flow inside the thin walled tube remain unknown the pressure flow data give some insight into the importance of their phase relationship and their net affect external to the pumping region.

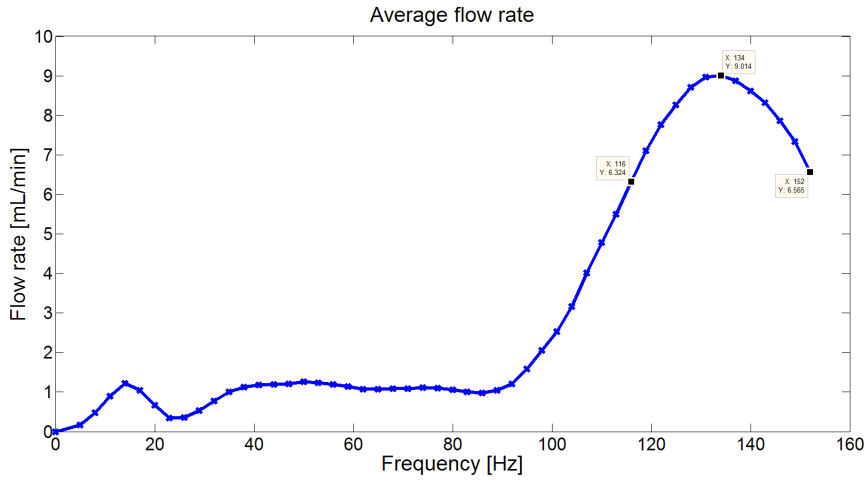

Figure 1.16: Shows a typical frequency response for the impedance pump and highlights three frequencies 116 Hz, 134 Hz, and 152 Hz.

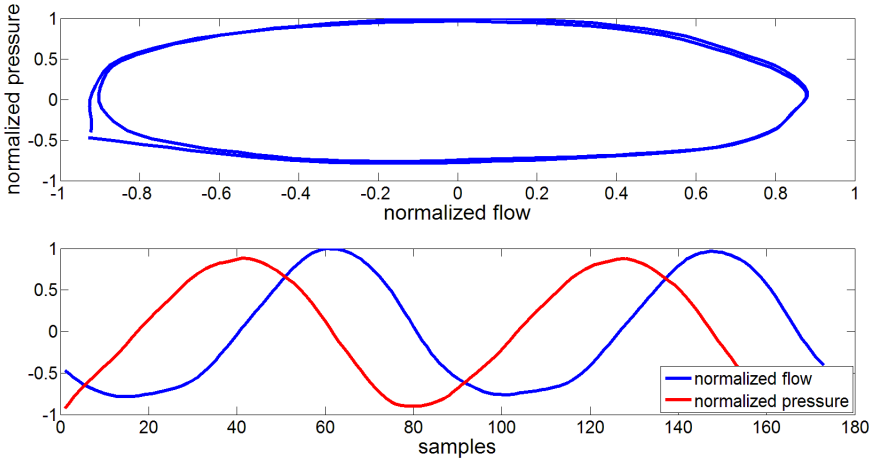

Figure 1.17: Pressure flow phase relationship at 116 Hz. Notice that in this case pressure precedes flow in phase generating an open P-Q loop.

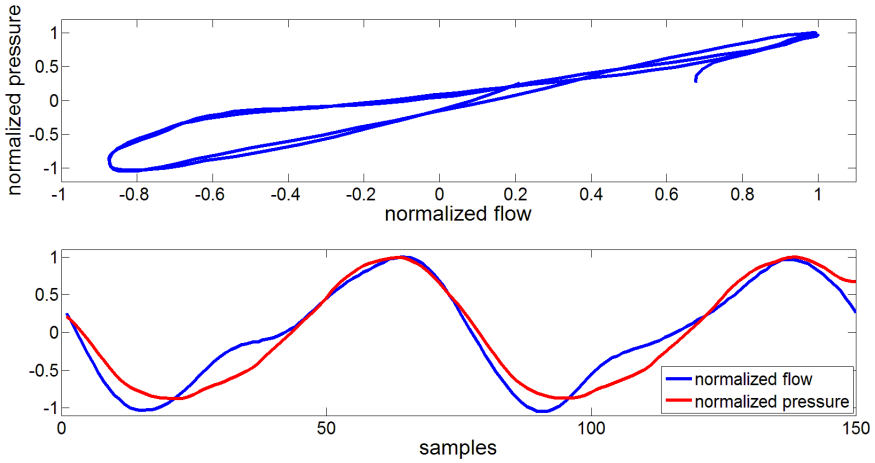

Figure 1.18: The pressure flow trace at 134 Hz, very close to resonance. Notice in this case pressure and flow are nearly in phase and the pressure flow loop collapses.

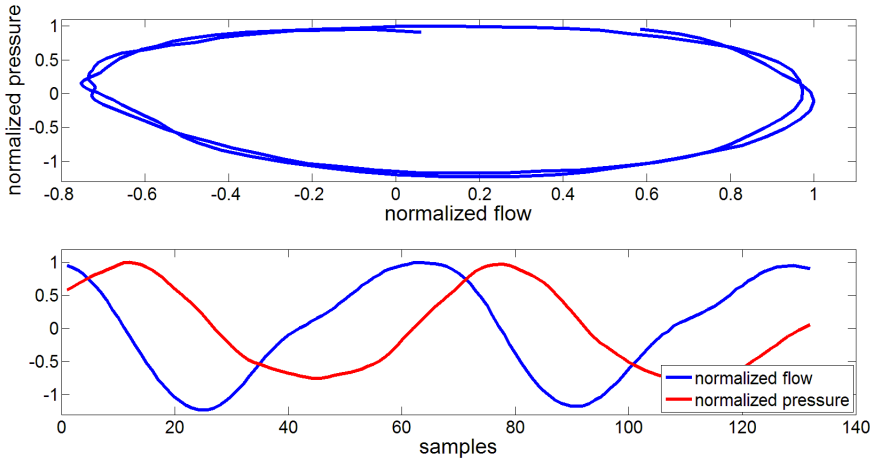

Figure 1.19: Pressure flow phase relationship at 152 Hz. Notice that in this case instead flow precedes pressure in phase once again generating an open P-Q loop.

1.4 Implementing the impedance pump on the microscale

1.4.1 Introduction

The basic concept of an impedance pump requires at least a single wave reflection site, a media functioning as the pump body to propagate the excitation as well as that the excitation occurs asymmetrically with respect to systemic impedance. Therefore when the question of scaleablity is posed there is nothing regarding the basic concept of the pump which is violated in going to smaller size scales. Additionally the proof of concept study presented in Micro Open Loop flow of Section 1.2.4.3 provided the evidence that using the impedance pump as a micropump was feasible. This evidence was further strengthened by observations of a purely biological system, the embryonic zebrafish which uses the mechanism of the impedance pump to move blood during the early post fertilization stages of cardiogenesis once diffusion alone has become inadequate to sustain development

The dimensionless parameter which describes the relative size of the inertial core relative to the boundary layer in a pulsatile flow is the Wormersley number (Wo). For the impedance pump the Wormersley number is taken in its original for given by:

$$\mathrm{Wo} = \mathrm{R}\sqrt{\frac{\omega}{v}} \tag{1.1}$$

where R is the channel radius, ω the rotational frequency in radians/sec, and ν the kinematic viscosity. Examining the Wo of both the 2 mm ID impedance pump and the roughly 2 cm ID impedance pump studied by Hickerson we can see that although these responses have different resonant frequencies due to the larger number of parameters which together produce the flow frequency response these flow responses occur over a similar range of Womersley numbers roughly Wo = 0 - 30. Therefore the argument could be made that given an actuator with sufficient frequency bandwidth a similar range of Wo numbers could be attained for a pump of a smaller characteristic inner diameter. For a 100 μm pump a Wo of 10 would require a frequency of roughly 6.3 kHz, well within range of the response of many common actuators.

1.4.2 Design considerations

Since ultimately the goal is to translate the pumping concept to working devices the benefits in scaling down the pump tend to be better viewed from a design standpoint. Smaller size dimensions favor the choice of actuators. The principle of the impedance pump is one of resonance small excitation amplitude can result in substantial flow output, however there is a threshold minimum displacement required to generate flow. Presumably this threshold, although it has not been measured experimentally, can be described by the relative ratio of that threshold displacement amplitude and the

characteristic internal diameter of the pump. This threshold has also been a resulting draw back to implementing the larger scale ($\sim$ 2 cm ID) impedance pump in a stand alone implantable device. The large dimensions limit the choice of actuators and frequency over which they are effective. The implications of this are seen in the experimental study by Hickerson[10] in that the frequency range was limited to below 20 Hz due to the speed of the motor. In her study an elegant mechanism composed of a series of gears with pins guided in a grooved slot to reciprocate the pinchers in a sinusoidal motion were designed to apply large displacements however due to issues of reliability and size such a mechanism would not be practical in an implantable device. Piezoelectrics and electrostatic actuation is impractical at those dimensions and electromagnetic mechanisms which apply such large displacements and can handle the inertia of actuation at high frequency tend to be extremely large, relative to the 1.9 cm by 15.2 cm pump. At smaller size scales below a millimeter there is better harmony between the apparent resonant frequency of the pump and that of common actuator materials, which affects the potential for maximal energy transmission to the working fluid.

As with any design problem there are tradeoffs regarding manufacturing and geometry at small size scales. Thin walled tubes elastic tubes are limited to wall thickness greater than 50 microns due the manufacturing processes involved in their fabrication. This has huge implications if one desires to create tubular impedance pumps at the microscale. In this case the wall thickness to inner diameter ratio is on the order of a factor or 10 greater than the pumps studied in Hickerson et al.[8], or Rinderknecht et al. [9] where the ratio is 0.041 and 0.025 respectively. However our hypothesis about the impedance pump concept tells us that there is nothing specific about the geometry of the wave propagating media. Additionally with the advent of microfluidics and manufacturing for Micro Electro Mechanical Systems (MEMs) many fabrication techniques are in existence which could easily be extrapolated to building a microscale impedance pump.

1.4.3 The effect of fluid viscosity on pump performance

Given that there was evidence that the impedance pump continued to function well at low Re there was a need to examine the effect of fluid viscosity on the performance on the pump. Two independent experiments were conducted. First the frequency response of the impedance pump was characterized versus varying viscosities from 1 cP to 40.55 cP. The viscosity was adjusted by varying ratio of glycerin to water by weight from 0 to 80%. The impedance pump tested was 27.0 mm in length and the excitation position was 3.89 mm from the right hand side wave reflection site. The pump had an inner diameter 2mm and a wall thickness of 780 μm. The excitation waveform applied to the pump was a sinusoid of 0.6 mm amplitude. The probe tip was lowered one half the amplitude of the excitation or 0.125 mm so that the tube is only completely open during the peak of the excitation cycle. The resulting frequency response can by seen in Figure 1.20. Flow from the right hand side wave reflection site to the left hand side wave reflection site is given as positive in

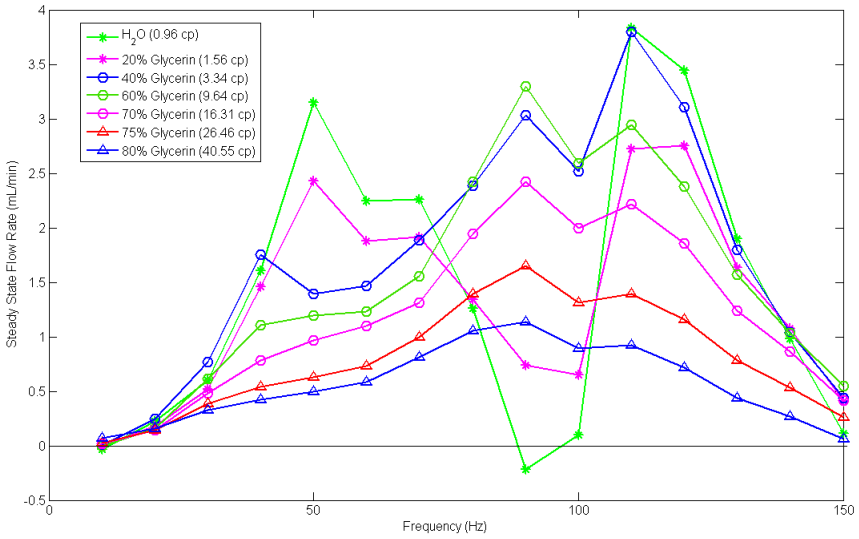

Figure 1.20: Flow frequency response of a 2 mm impedance pump scanned in increments of 10 up to 150 Hz. The individual color traces show the response of the pump to increasing fluid viscosity.

Figure 1.20. Given the frequency response of the 0.96 cP case it is easy to recognize the resonant peaks of 3.1 mL/min at 50 Hz and 3.8 mL/min at around 110 Hz as well as the small reversal of 0.3 mL/min at 90 Hz. Observing the frequency response the affect of increasing viscosity has an averaging-like affect of the frequency to frequency response of the pump. After only an increase from 0.96 cP to 1.56 cP in viscosity the flow reversal at 90 Hz is completely eliminated. The most prominent flow peak, at 110 Hz, continues to dominate until 26.46 cP or 60% glycerin where is it then overshadowed by the emergence of a new peak at 90 Hz. When this frequency response is plotted against the Womersley number and the flow output is nondimensionalized by half the rate of the volume displaced by the pinchers as suggested by Thomann (1978) and adopted by Hickerson et. al. the respective frequency responses are compacted as shown in Figure 1.21. Otherwise the plots display similar features to the dimensional frequency response. Next an experiment was carried out with the same setup as that presented in the micro open loop Section 1.2.4.3 to attempt to establish some lower end Reynolds number limit to where the impedance pump principle ceases to function. Three different pumps were tested whose geometries are summarized in Table 1.4.3. The current input to the electromagnetic cantilever style actuator was 84.3 Hz sinusoid with an amplitude of 32 mA.

The plot in Figure 1.22 shows that the impedance pump at 60 times the viscosity of water still produces a flow rate of 3.42 μL/min, or steady Reynolds number of 0.02. Scaling this back in terms of the dimensionless parameter the Reynolds number this represents an effective inner diameter of

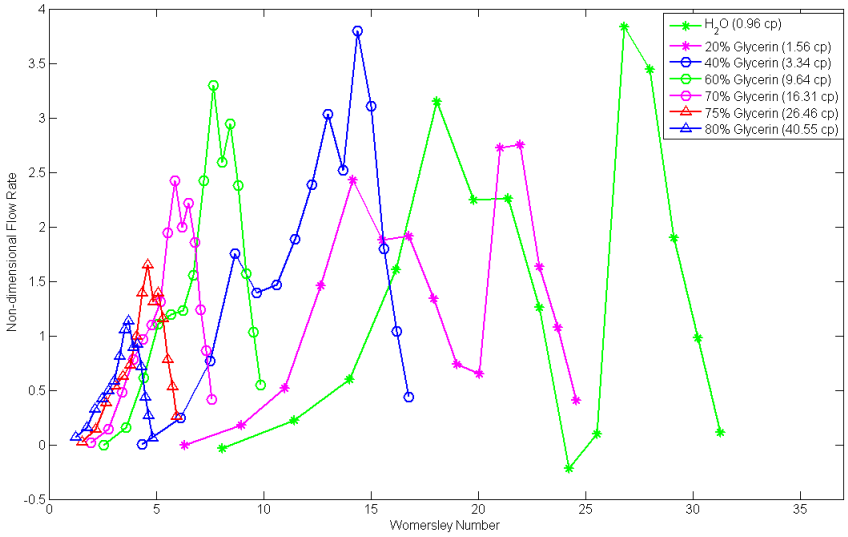

Figure 1.21: The same plot as Figure 1.20 but non dimensionalized according to the methods of Thomann 1978 and plotted versus the Wo.

	Rigid coupling		Elastic Tube			
Pump	ID [μm]	Wall [μm]	L [mm]	ID [μm]	Wall [μm]	*EL [mm]
1	250	50	8.42	250	50	1.56
2	400	35	8.10	300	150	1.40
3	400	35	10.52	300	150	2.11

Table 1.3: Summarizes the parameters of the three pumps used in the micropump viscosity study. * **Note**: EL denotes excitation location as defined from the left hand side wave reflection site.

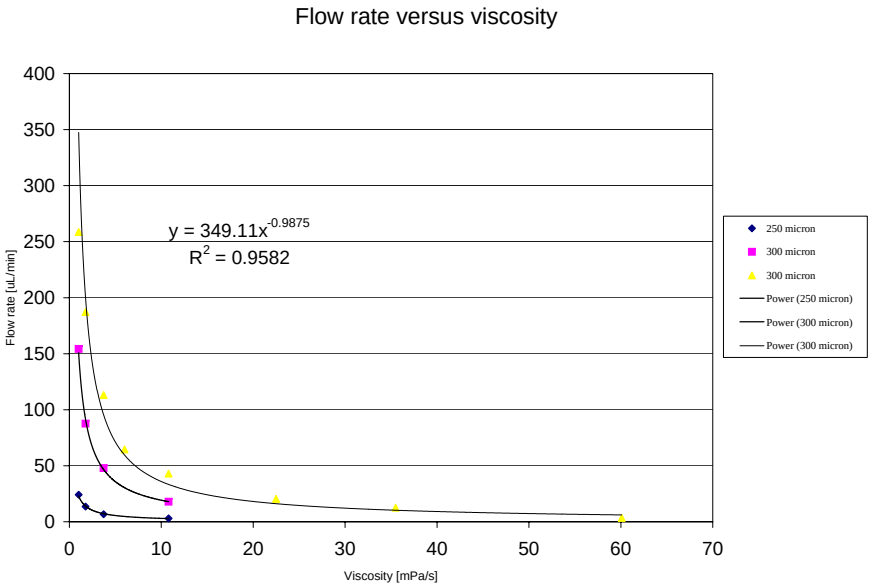

Figure 1.22: Shows the output flow rate of three impedance pumps at a frequency of 84.3 Hz versus increasing fluid viscosity.

approximately 5 μm.

1.4.4 Conclusion

Construction of the characterization system and the proof of concept experiments based around the electromagnetically actuated impedance pump were able to lay the ground work to consider the impedance pump for applications other than strictly a biomedical device for active stents and shunts. The favorable response of the impedance pump to increases in fluid viscosity shows that although the output is attenuated the impedance pump concept still functions down to Reynolds numbers of 0.02. Considering the impedance pump as a micropump opens many new avenues for exciting applications ranging from Lab-on-Chip diagnostics to microscale thermal management.

1.5 Microfluidic platforms and applications

1.5.1 Impedance pumps in Lab-on-chip microfluidics

Microfluidics offers a unique opportunity to observe biological and chemical events in an environment which can easily be controlled and manipulated. Since the early 1990's scientist and researchers have discovered that microfluidic devices can be useful in a plethora of applications ranging from thermal management systems for cooling microprocessors to screening and analysis for pharmaceutical discovery, polymerase chain reaction (PCR), and protein crystallization. As demand drives integrated microfluidic systems to pack increasingly more components per unit area, microfluidic systems must be able to perform operations with smaller volumes and on shorter time scales allowing a larger number of operations to occur on a single chip. Since integration is a key issue and a limiting one in the overall success of microfluidic components, in addition to being effective and space conservative, microfluidic components must easily operate in a planar format, where integrated systems are built up from a series of layers. This format creates a synergy between all microfluidics components as well as agrees with the next obvious step in large scale integration, 3-D fabrication.

Given the basic principles of the impedance pump, there is no required geometry therefore standard soft lithography offers us a fabrication technique to begin producing impedance pumps in a planar format which can easily be prototyped with other microfluidic components within the context of Lab on Chip diagnostics.

A variety of different impedance pumps have been fabricated in polydimethylsiloxane (PDMS) microchips for applications ranging from heat transfer to blood glucose sampling. An example of such devices can be seen in Figure 1.23. The device on the left was made to demonstrate that the impedance pump principle could easily be implemented within the context of a closed microfluidic system. The device on the right was made as a sample diagnostics demonstration for sampling a

biological fluid such as blood. Here the fluid to be sampled could be drawn in through the inlet and stored in a series of reservoirs which can be opened and closed through a series of valves. One of the problems with Lab on chip sampling devices is the volume required to form the sampling line, which in the case of a glucose monitoring device would most likely the hollow body of a needle. From sample to sample this line needs to be flushed to ensure accurate sampling such that no residual stagnant fluid is left in the sample line between samples. The impedance pump lends itself well to this problem in that by taking advantage of the bidirectionality of the impedance pump a single pump can be used to reverse the flow flushing the sampling chambers to prevent coagulation and ensure that a fresh sample was stored. A second pump was also placed on the device to allow previously stored samples to be transported to other areas on the chip for diagnostic operations such as measuring HCO_3-, pH or other physiological markers. Adhering to the basic principles of having a wave reflection site, wave carrying media and an asymmetric excitation location with respect to systemic impedance a microscale impedance pump on a chip was constructed out of PDMS. In this case the wave carrying media is created not by a tube but by a flexible membrane. The pump dimensions are 20 mm in length by 3mm in width with a 200 μm channel depth. Wave reflection sites are created by two affects: one an abrupt geometrical length change as the 3mm pump width couples to the 300 micron flow channel as well as thickening of the PDMS material over the whole boundary to reflect any energy carried by at the center of the propagating surface wave. If the latter affect was not addressed, the layered fashion of PDMS manufacturing would result in an entire microfluidic channel has an upper wall which was free to deflect with changes in pressure and hence could remove energy from the pumping process which could otherwise be rectified and used to drive the flow. The micro impedance pump on the left in Figure 1.23 was tested using the perpendicular coil arrangement specified in Section 1.2.3.1. The NdFeB magnet was positioned on top of the pump and actuated using a 119 Hz square wave with 16 mA offset and 60 mA amplitude at a position of 4.6 mm from the right hand side wave reflection site. The flow output produced by the microimpedance pump was 16 μL/min.

1.5.2 Impedance pumps in rigid systems

Recently we have demonstrated that these principles work equally well in more rigid systems. Early prototypes have been manufactured using standard micro machining techniques from brass and aluminum however can easily be adapted to silicon based fabrication. A picture of a metallic micro impedance pump prototype can be seen in Figure 1.24. Preliminary studies have yielded flow rates of 190 μL/min.

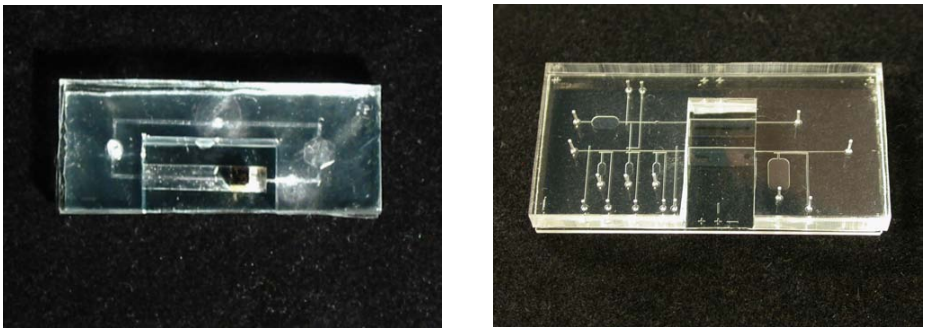

Figure 1.23: Two different PDMS devices with integrated microimpedance pumps. The device on the left was built to demonstrate the ability to generate flow using microimpedance pump in a closed loop microsystem the second was built to demonstrate a series of microimpedace pumps implemented in complex microfluidic system for sampling and diagnostics.

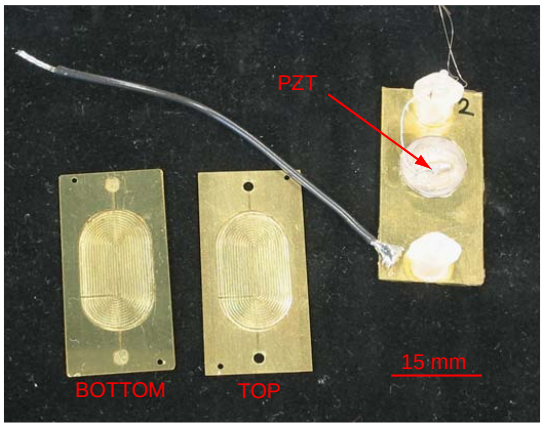

Figure 1.24: A picture of the inside of a rigid micro impedance pump. The material is brass. A small pocket has been machined out to form the body of the pump. Wave reflection sites are created by the change in geometry. Excitation still occurs asymmetrically with respect to the length of the pump body.

1.5.3 A case study: Optimization of microscale heat transfer

1.5.3.1 Introduction

Understanding the mechanisms of thermal transport at the microscale is important to applications ranging from chip level cooling of microprocessors and power amplifiers (PAs) to effective rapid cycling of polymerase chain reaction (PCR) for DNA amplification. In these applications the heated area is usually along a single planar surface within a microchannel. Maximal uniform heating or cooling of the working fluid is often critical to effective operation. The most common system for studying heat transfer in microchannel heat sinks involves a surface with constant heat flux over which an integrated heat sink is used to remove heat. These systems are either open loop or closed loop referring to whether flow occurs within a closed circuit or between two independent thermal or fluid reservoirs. In addition to the flow parameters such as pressure drop and flow rate, three temperatures are usually monitored: the inlet temperature, outlet temperature and the die temperature (chip surface temperature.) Many studies have been undertaken to optimize the geometry of microchannel heat sinks [19]. As a result, much of the trend in microchannel heat sinks has been to ignore the fluid dynamics, electing to enhance heat transfer by means of a pure decrease in size of the microchannels, which increases surface area to volume ratio thus reducing the effects of the thermal boundary layer. The price paid for this, however, is a drastically increasing pressure drop across the heat sink, which leads to costly packing and safety issues in addition to a thermal management system which requires a large amount of input power. Pulsatile flows circumvent this problem, because they can manipulate the thermal boundary layer by increasing the interfacial area between the hot and cold fluid, with no need to change the channel geometry.

1.5.3.2 Background

Along these lines many methods to enhance single-phase heat transfer devices have been proposed, such as developing flow, swirl flow, vibration, secondary flow and mixing; however very few of these methods have been implemented experimentally, or systematically explored, at the microscale. Therefore there is a large body of relatively unexplored thermal transport problems. Heat transfer augmentation methods have been reviewed by a variety of authors including Tao et al. [20]. Tao divided heat transfer augmentation methods into three mechanisms: decreasing the thermal boundary layer, increasing flow interruptions and increasing the velocity gradient near the heated surface. Many of these flow augmentation methods can be achieved through pulsatile flows.

Pulsatile flows have been explored in a variety of contexts for enhancing heat transfer. Numerical studies by Moschandreou and Zamir[21] and Kim et al.[22] have suggested that oscillatory flows can enhance convective heat transport by as much as 20%. A 50% increase in heat transfer enhancement for pulsatile flows with flow reversals[23]. Analogous experiments have been performed on the

large scale on oscillating cylinders in cross-flow. The experimental results performed by Pottebaum show that the wake mode created by vortex shedding from a cylindrical body in cross-flow plays a significant role in determining heat transfer coefficient; this work demonstrated that an oscillating cylinder in cross-flow can augment heat transfer coefficients by as much as 8 times[24]. These studies reveal the importance of flow/structure interaction in aiding in convective heat transfer, given that heat transfer from the cylinder into the surrounding fluid can be significantly enhanced by modifying the flow field to augment the transport of heated fluid out of the thermal boundary layer. We find merit in exploring the mechanisms of heat transfer augmentation in these pulsatile flow systems, when considering that even a 50 % increase in the heat transfer coefficient for pulsatile flow conditions translates into an increase in the dimensions of a channel heat sink equivalent to a reduction in pressure drop by a factor of 3 or more; effects at the microscale may be even more substantial.

1.5.3.3 Experimental apparatus

Since the aim of this experiment was to investigate the effect of pulsatile flow profiles on heat transfer in microscale geometries. Preliminary studies were conducted to optimize the heat transfer in a custom designed micromachined heat sink with a channel depth of 100 μm. The heat sink is attached to the backside of a Riedon Inc. TF1218H-A 100 Ω power resistor with a supply voltage of 20 V in order to dissipate a heat flux of 4 W/cm2. The inlet and outlet of the heatsink were connected within the characterization flow loop described in Figure 1.13. Thermocouples were installed on the inlet to the heatsink, outlet to the heat sink and in the thermal junction between the heatsink and the sinking surface of the power resistor. Downstream of the outlet of the micromachined heatsink was a large water bath which functioned as thermal reservoir to maintain constant inlet temperature to the heatsink as well as allow the optimization to work over long time periods. The temperature of the incoming water from this reservoir is monitored by the inlet heatsink thermocouple. The difference between the inlet and outlet thermocouple gives a measurement of the average thermal power removed by the fluid flow. The junction thermocouple allows us to monitor the junction temperature, a critical temperature for establishing the thermal resistance to heat flow into the working fluid.

The pump used in this study was a 2 mm ID impedance pump with a 780 μm wall driven by the characterization system described Figure 1.13. The impedance pump was 14.87 mm in length with a excitation location of 2.52 mm from the left hand side wave reflection site. The frequency input was a sine wave that was allowed to vary from 10 -150 Hz and amplitude limited to the range of 0.1 to 0.5 mm. No electrical offset was applied to the waveform however a mechanical offset of 1.397 mm was applied through the z-traverse. The heater was activated for 3 secs before the pump was activated.

To explore the large parameter space comprised of the pump and heatsink system an optimizer based on an evolutionary algorithm was employed. In this study the optimizer sought to maximize the temperature difference between the inlet and outlet bulk fluid temperatures of the heat sink, while minimizing the average flow rate, a linear combination of the flow rate and the inverse of the temperature difference are minimized. To allow the optimizer to run for long periods of time and preserve the initial conditions of the experiment, if the amplitude frequency choice of the optimizer produced insufficient flow to prevent the fluid in the heatsink from boiling, the point was discarded. After every run a cooling cycle was applied to lower the heatsink temperature to within 99% to that of the inlet thermocouple reading.

1.5.3.4 Results and Discussion: System specific optimal points for heat transfer

The performance of the impedance pump, similar to the pulsatile flow heat transfer problem, varies with the excitation frequency and amplitude. This combination of systems results in an optimal region for heat transfer, which is the intersection of two regions: one which results in efficient heat transfer characteristics, and another which contains optimal points which produce effective flow performance for the pump. The left part of Figure 1.25 shows a contour plot of the optimal region, found by the optimizer. The plot on the right in Figure 1.25 shows the temperature difference produced by one point belonging to the converged solution of the optimizer for the pump/heat sink system compared to the temperature difference which results from steady flow. The mean flow rate for both the steady and oscillatory cases is 8.37 mL/min. The excitation frequency and amplitude for the pulsatile flow case are 122 Hz and 0.37 mm, respectively.

Examining the plot on the right of Figure 1.25 it is noticeable that the pulsatile flow case is more effective at removing heat versus the steady case. Comparing the ΔT of this point to the steady flow case there is a 25 % increase in ΔT for the optimal pulsatile flow with a negligible change in system pressure (760 Pa steady/768 Pa pulsatile). These optimal points are largely affected by the frequency response of the pump due to the fact the points insufficient to cool the heatsink are discarded however a larger frequency and amplitude domain still exists. Unfortunately the brass heatsink did not allow visual access therefore it is difficult to determine the exact physics responsible for the increase however such points providing enhanced heat transfer do exist under pulsatile flow conditions.

1.5.3.5 Conclusion

An experiment was conducted to examine whether pulsatile flow can be used as a method of heat transfer enhancement in microchannel heatsinks. The frequency and amplitude space of heat transfer were examined for the combination system of an impedance pump and a custom machined brass microchannel heatsink to determine whether pulsatile flow points existed which provided enhanced

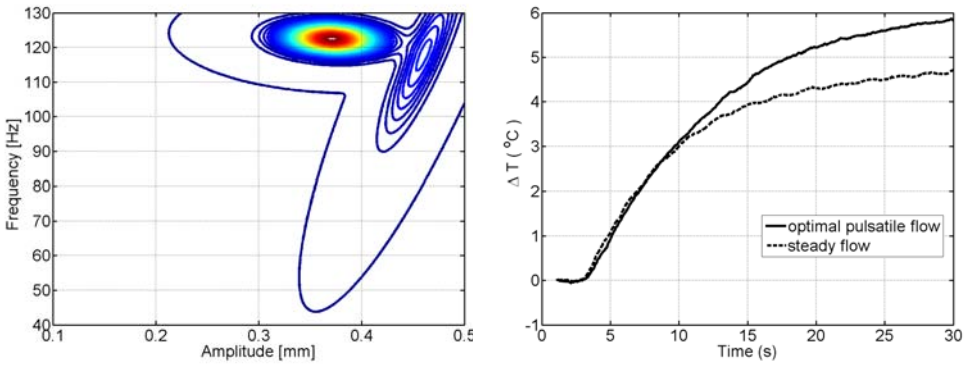

Figure 1.25: Shows preliminary data, on the left is the contour plot of the distribution of optimal points found by the optimizer. The plot on the right compares the optimal point of the contour plot on the left to steady flow. For both cases the mean flow rate is 8.37 mL/min the change in pressure drop was negligible.

heat transfer for the pump-heatsink system versus steady flow. In order to search the large parameter space an evolutionary optimization routine was employed. The cost function looked for points where heat transfer was maximized while the power input to the fluid was minimized. One of the predicted optimal points, a frequency of 122 Hz and 0.37 mm amplitude, shows a 25% increase in the temperature difference inlet to outlet versus steady flow of an equal mean flow rate.

1.6 Summary

The impedance pump functions through dynamic wave interactions allowing a pressure gradient to be created across the ends of the pump. The concept has been shown to require the presence of one or more wave reflection sites functioning as boundaries located along a compressible section as well as an excitation occurring asymmetrically with respect to systemic impedance. To tackle the huge parameter space of the pump the characterization system was constructed to measure time resolved pressure and flow in order to provide an understanding of how these parameters influence their interaction and how these dynamics give rise to flow. As a result many of the studies invovled in the characterization of the large scale impedance pump by Hickerson in her thesis were able to be repeated at millimeter size scales and smaller. These experiments include:

1. Measurement of the flow response of the impedace pump to open loop and closed loop flow conditions.

2. Observation of the symmetry of the flow reponse to excitation location.

3. Pressure-flow loops describing the contribution of potential work to the flow.

4. Response of the pump to increases in fluid viscosity.

5. Response of the flow output to transmural pressure.

The concept of the impedance pump was demonstrated to be scaleable down to a few hundred microns and tested under increased viscosity demonstrating that the concept is robust to the dominance of viscous forces at the microscale. Microscale impedance pumps were then fabricated using current microfabrication and micromachining techniques demonstrating that the impedance pump concept can drive fluid in microfluidic systems. The basic concepts were then extrapolated further to create impedance pumps composed entirely of rigid materials. This work opened the door to consider impedance pumps in a wide range of applications spanning micro implantable pumps for treating glaucoma and hydrocephalus, to lab-on-chip diagnostics or even for applications in drug delivery and microscale heat transfer.